Phononic and optical behavior of reactive-sputtered Cr_2O_3 thin films for infrared optoelectronics

N. ROMCEVIC[1], M. CURCIC[1,*], J. PESIC[1], N. PAUNOVIC[1], S. PETROVIC[2], U. RALEVIC[1], M. ROMCEVIC[1], M. GILIC[1]
[1]*Institute of Physics Belgrade, Pregrevica 118, 11080 Belgrade, Serbia*
[2]*Institute Vinca, P.O. Box 522, 11001 Belgrade, Serbia*

Cr_2O_3 is a promising semiconducting material for applications in optoelectronics devices, e.g. in novel differential photodetectors. Cr_2O_3 thin films with varying thickness were deposited on glass by reactive magnetron sputtering under different oxygen partial pressures. AFM, Raman and far-infrared (FIR) spectroscopy were used to correlate deposition conditions with film structure and optical response. The FIR reflectivity was interpreted using a film–substrate numerical model, while phonon assignments were supported by first-principles DFT calculations. A distinct surface optical phonon (SOP) mode was identified, underscoring the potential of Cr_2O_3 thin films for infrared optoelectronic and photodetector applications.

(Received December 25, 2025; accepted June 2, 2026)

Keywords: Cr_2O_3 thin films, Optical coatings, Surface optical phonon, Reactive sputtering, Density functional theory, Far-infrared spectroscopy

1. Introduction

Semiconductor materials, particularly in the form of thin films, have become indispensable in contemporary electronic and optoelectronic technologies due to their broad range of applications and high adaptability to specific functional requirements. Their widespread adoption is largely driven by the feasibility of cost-effective fabrication methods, which make them suitable for both commercial device integration and fundamental investigations in solid-state physics [1].

In particular, nanoscale thin films offer unique advantages for the precise tuning of electronic and optical properties, enabling researchers and engineers to design materials with tailored characteristics. By carefully controlling synthesis parameters—most notably, the film thickness—it is possible to manipulate the band gap, thereby directly influencing the absorption spectrum, peak absorption values, and overall electronic behavior of the material. Such tunability facilitates the development of application-specific solutions across a range of advanced technological platforms [2].

A wide range of inorganic semiconductors with wide band gaps—such as GaN, ZnO, TiO_2, and GaP—have become foundational materials in the field of optoelectronics, owing to their high band gap values and ability to operate under high-energy conditions, including elevated temperatures and intense electromagnetic radiation [3–5]. Their chemical stability, resistance to degradation, and tunable optical and electronic properties through structural and morphological modifications make them suitable for a broad spectrum of applications, ranging from LEDs and lasers to UV detectors and transparent conductive layers. In this context, the study by Wang et al. [6] further expands this landscape by introducing Cr_2O_3 thin films as a promising addition to this class of advanced materials. The authors emphasize their strong photoresponse and sensitivity to optical excitation, suggesting great potential for detectors, optical switches, and other functional components in optoelectronic systems. Moreover, Cr_2O_3 films demonstrate the ability to operate in extreme conditions, distinguishing themselves as a robust and reliable platform for developing the next generation of high-performance devices. Their properties can be further engineered by optimizing the deposition process, making them highly flexible materials for nanoelectronics and photonics.

Compared with more mature wide-band-gap oxide platforms such as ZnO-, TiO_2-, SnO_2-, and In_2O_3-based systems, p-type oxide semiconductors remain considerably less developed because hole transport is generally limited by the localized O 2p-derived valence band. In this broader context, chromium-based oxides, and Cr_2O_3 in particular, have attracted growing interest owing to their chemical stability, wide-band-gap character, and potential for p-type functionality. Recent studies further indicate that Cr_2O_3 research is moving beyond basic materials synthesis toward device-relevant structures, including oxygen-pressure-controlled magnetron-sputtered thin films, Cr_2O_3/n-Si heterojunctions employing Cr_2O_3 as a hole-selective layer, and p-type Cr_2O_3 films evaluated for Schottky-diode applications. These developments support

the view that Cr_2O_3 is a promising complementary oxide platform for future optoelectronic architectures, especially where chemical robustness and controlled thin-film growth are required [7-10].

Cr_2O_3, as the only stable oxide form of chromium under ambient conditions, is a material of particular importance in contemporary research on functional oxides. Its strong absorption in the visible region of the spectrum, with characteristic absorption maxima around 640 nm and 570 nm [11], indicates a significant interaction with light, making it suitable for optoelectronic applications that require selective or enhanced light absorption. Thanks to its wide band gap and high chemical stability, Cr_2O_3 is classified among key wide band-gap transition metal oxide semiconductors for the development of advanced electronic and optoelectronic components. Its properties are especially valued in applications such as absorbers in solar thermal systems, where it effectively collects and converts solar energy, as well as in protective coatings used under extreme working conditions, where a combination of optical transparency, corrosion resistance, and mechanical durability is required [12, 13]. Due to these characteristics, Cr_2O_3 is increasingly recognized as a material with great potential for the next generation of durable and high-performance optoelectronic devices, including photosensitive sensors, protective layers in the solar industry, and components in light detection and conversion devices.

Phonon studies enable precise engineering of material properties at the atomic level, which is crucial for designing next-generation optoelectronic devices with better performance, efficiency, and versatility [14]. For example, materials with tailored pho-non properties can achieve better thermal conductivity or thermal isolation, improving the efficiency and longevity of optoelectronic devices [15]. This is especially true for crystals of reduced dimensions, like thin films, where a unique phonon mode—known as the surface phonon mode—emerges in the frequency range below the bulk longitu-dinal optical phonon frequency (ωLO) [16,17]. For real crystals with limited dimensions, surface modes and size effects become increasingly pronounced, adding complexity to the normal modes found in an infinite lattice. As the crystal dimensions shrink further, only the surface phonon mode remains prominent, dominating the vibrational behavior [16-18].

In this study, we present both experimental and theoretical analyses of the phonon characteristics of Cr_2O_3 thin films synthesized via the reactive sputtering technique. Sample characterization was conducted using atomic force microscopy (AFM), while the structural and optical properties were investigated through Raman spectroscopy and far-infrared spectroscopy. Density functional theory (DFT) was employed for accurate phonon mode assignments, enhancing our understanding of the phononic behavior of these films.

2. Methods and materials

The Cr_2O_3 thin films were fabricated on glass substrates in Balzers Sputtron II system. Depositions were done in DC (direct current) reactive sputtering operating mode. The base pressure in the chamber was 7×10^{-6} mbar, all depositions were per-formed at ambient temperature with deposition time of 20 min. Oxygen partial pressure was changed from 3 over 5 to 7×10^{-4} mbar. The obtained film thicknesses, measured by a profilometer type Talystep, were 60, 270 and 340 nm, respectively, indicating on strong dependence of deposition rate versus oxygen partial pressure. By changing oxygen partial pressure from 3 to 5×10^{-4} mbar the thickness of deposited film (therefore depo-sition rate) slightly increases from 270 to 340 nm. Large drop-in of deposition rate was registered for the highest value of applied oxygen partial pressure (Fig. 1). The reason for a significant decrease in the deposition rate of layers can be the accelerated oxidation of the Cr target - which leads to a reduction in its sputtering rate, as well as the increased number of collisions between sputtered Cr particles on their way to the substrate.

Although reactive sputtering is a scalable thin-film deposition technique, Cr_2O_3 growth remains highly sensitive to oxygen partial pressure and target oxidation effects, which may influence deposition rate, stoichiometry, and run-to-run reproducibility.

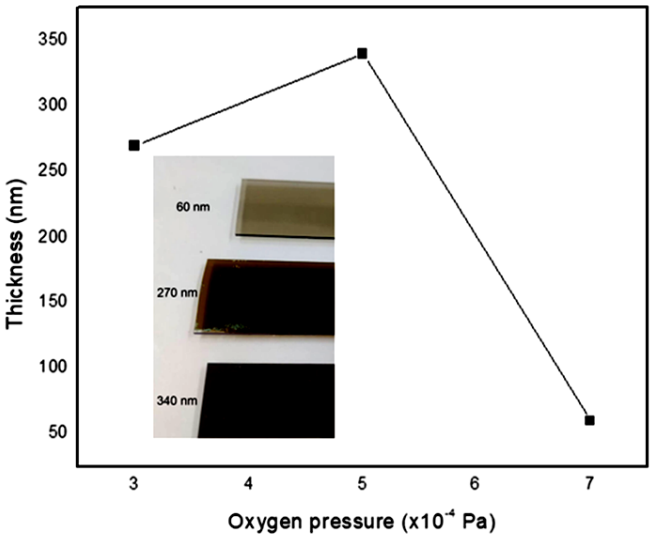

Fig. 1. The effect of oxygen partial pressure on the thickness of chromium oxide films; inset: image of the films deposited on the glass substrate

The surface morphology of three Cr_2O_3 thin films with varying thicknesses was examined using atomic force microscopy (AFM). AFM measurements were conducted on an NT-MDT NTEGRA Prima system, employing tapping mode with NSG01 probes. All measurements were performed under ambient conditions.

Micro-Raman spectra were acquired in a backscattering configuration using a TriVista 557 spectrometer, equipped with a nitrogen-cooled charge-coupled device (CCD) detector. The 532 nm line of a Ti: Sapphire laser served as the excitation source, with a laser power of 50 mW.

Far-infrared (FIR) reflectivity measurements were conducted at room temperature using a BOMEM DA-8 Fourier-transform infrared (FTIR) spectrometer. A Hyper beamsplitter and a deuterated triglycine sulfate (DTGS) pyroelectric detector were utilized to cover the wavenumber range of 60 to 670 cm^{-1}.

In the present work, the focus was placed on the correlation between oxygen partial pressure, film thickness, and phononic/optical response, while large-area uniformity and batch-to-batch reproducibility were not systematically investigated and remain important topics for future technological optimization.

3. Results and discussion

3.1. Atomic force microscopy

Fig. 2 displays three-dimensional topographic images of the samples. An im-provement in film quality is observed with increasing thickness, as anticipated. For the thinnest film, at 60 nm, the surface exhibits irregularities with numerous clusters av-eraging around 1.66 nm in height. As film thickness increases, the surface morphology becomes more uniform and homogeneous.

Characteristic quantitive AFM parameters of chromium oxide thin films are summarized in Table 1, with the abbreviations defined as follows:

Ra (Average Roughness): the arithmetic average of the absolute deviations of surface heights from the mean height, providing an overall measure of surface roughness;

RMS (Root Mean Square Roughness): The square root of the mean of the squared deviations of surface heights from the mean height, giving more weight to larger devi-ations and highlighting significant surface irregularitie;

Skk (Skewness): A measure of the asymmetry of the surface height distribution. Positive values indicate surfaces dominated by peaks, while negative values suggest surfaces dominated by valleys. A value close to zero implies a balanced distribution.

Overall, the sample surfaces are relatively flat, yet they feature bright protrusions and dark depressions that contribute to a minor surface roughness of a few nanometers. This subtle texture indicates a controlled roughness profile, reflecting consistent film growth while maintaining the surface stability required for advanced applications.

The non-monotonic variation of the average height and Skk values reflects the combined influence of oxygen partial pressure, deposition rate, and island coalescence during film growth, rather than a simple thickness-dependent trend.

Table 1. AFM parameters for Cr_2O_3 thin film samples

Sample	**60 nm**	**270 nm**	**340 nm**
Average height (nm)	1.66	2.05	1.80
Ra (nm)	0.31	0.44	0.48
RMS (nm)	0.73	0.68	0.66
Skk	18.21	2.84	1.65

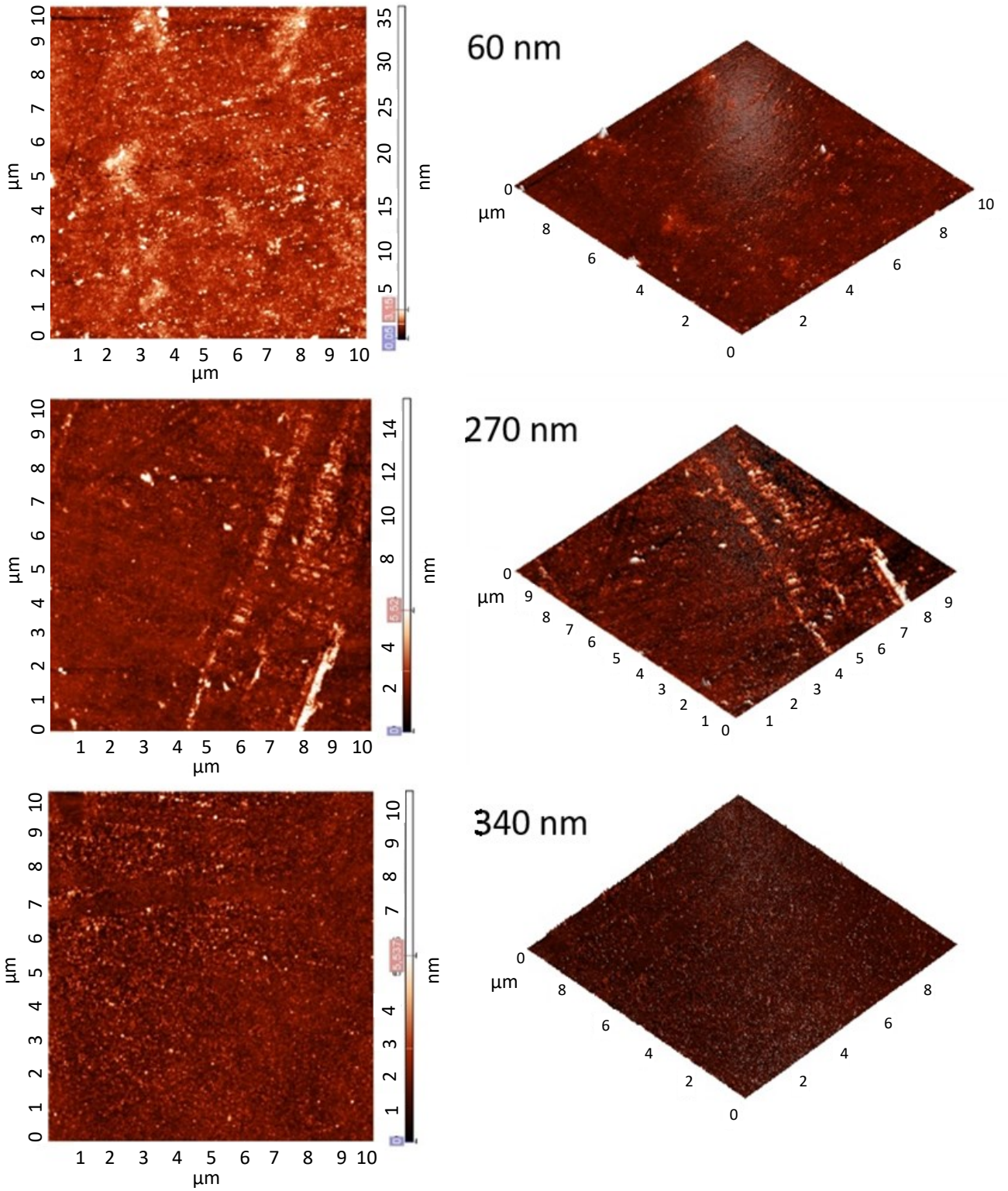

Fig. 2. AFM images of the Cr_2O_3 films deposited on glass substrate for different thicknes sample (colour online)

3.2. DFT calculations

To thoroughly analyze the far-infrared and Raman spectra of the Cr_2O_3 thin film samples, we initially conducted a DFT (density functional theory) analysis. These calculations were performed using the Quantum Espresso software package [19], employing PAW pseudopotentials [19, 20] in conjunction with the Perdew-Burke-Ernzerhof (PBE) exchange-correlation functional [21] and the DFT + U approach by Liechtenstein et al. [22], with a correlation parameter U=3.7 eV. For the calculations, cutoff energies of 60 Ry for the electron

wavefunction and 460 Ry for the charge density were selected. The k-points were sampled using a Monkhorst-Pack grid, employing a 12×12×12 Gamma-centered configuration. Prior to phonon calculations, the lattice parameters and atomic positions within the unit cell were relaxed to reach the minimum energy state, using the BFGS algorithm. To enhance accuracy, van der Waals interactions were accounted for using the Grimme-D2 correction. Phonon frequencies at the Gamma point were then calculated using the linear response method available in Quantum Espresso. The Cr_2O_3 unit cell structures used in the DFT analysis are depicted in Fig. 3, and Table 2 presents the results obtained from this analysis [23].

Table 2. DFT-calculated mode frequencies for Cr_2O_3

No.	ω [cm^{-1}] Calculated DFT	ω [cm^{-1}], Raman measurements. This experiment	ω [cm^{-1}], FTIR measurements. This experiment	Mode symmetry
1.	204.9	201		E_g, Raman active
2.	301.8			A_{2g}
3.	308.8	308		E_g, Raman active
4.	326.7	347		E_g, Raman active
5.	342.5		340	E_u, IR active
6.	351.4	382		A_{1g}, Raman active
7.	377.9		379	E_u, IR active
8.	422.9		424	A_{2u}, IR active
9.	462.8			A_{1u}
10.	469.7			A_{2g}
11.	524.1			E_g, Raman active
12.	551.9		545	E_u, IR active
13.	586.4	543		A_{1g}, Raman active
14.	587.7			A_{1u}
15.	636.9		635	A_{2u}, IR active
16.	682.1	631		E_g, Raman active
17.	714.9		690	E_u, IR active
18.	734.8			A_{2g}

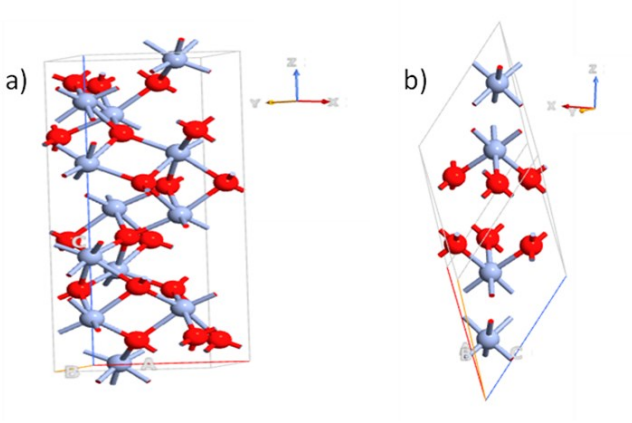

Fig. 3. The conventional (a) and the primitive (b) unit cell of Cr_2O_3 (colour online)

3.3. Raman spectroscopy

Fig. 4 presents the Raman spectra of Cr_2O_3 thin films with varying thicknesses on glass substrates. Among these, the 270 nm thick sample exhibits the highest quality spectrum. Mode assignments derived from DFT analysis are also indicated in Fig. 4, and the specific results are summarized in Table 2. Our experimental findings align well with the DFT calculations and are consistent with previously published results and theoretical calculations by other researchers [24-29].

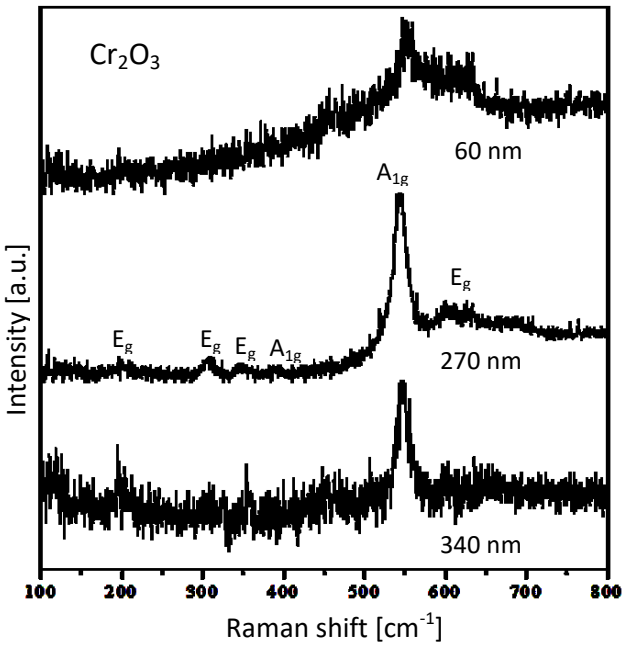

Fig. 4. Raman spectra of Cr_2O_3 thin films with thickness of 60 nm, 270 nm and 340 nm on glass substrate

3.4. Far-Infrared spectroscopy

Thicknesses of our films are in a range from 60 nm to 340 nm, so reflectivity spectra contain information about Cr_2O_3 films together with information about substrate. A representative schematic of our layered structure is presented in Fig. 5. Medium 1 is air, medium 2 is the thin film Cr_2O_3 crystal layer and medium 3 is substrate glass, with dielectric functions ε1 (ε1=1), ε2 and ε3, respectively.

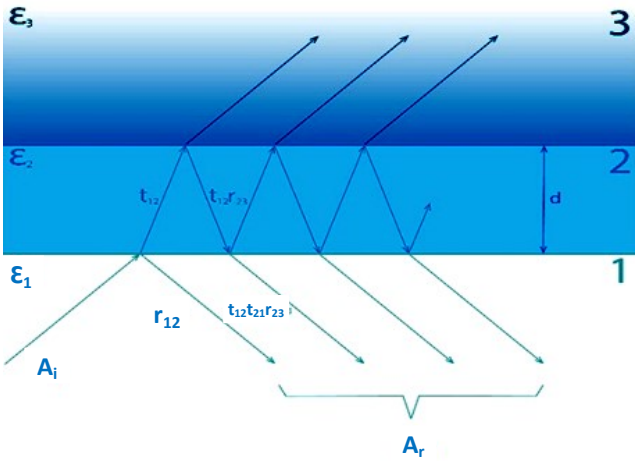

Fig. 5. Schematic presentation of a three-layer structure (colour online)

One can now write [16, 26]:

$$R_A = \frac{A_r}{A_i} = \frac{r_{12}e^{-ia} + r_{23}e^{ia}}{e^{-ia} + r_{12}r_{23}e^{ia}} \quad (1)$$

where

$r_{ij} = (n_i - n_j)/(n_i + n_j) = (\sqrt{\varepsilon_i} - \sqrt{\varepsilon_j})(\sqrt{\varepsilon_i} + \sqrt{\varepsilon_j})$

describe Fresnel coefficients, A_i and A_r represent amplitudes of incident and reflected beams, n is complex index of refraction, ε is the dielectric constant and $\alpha = 2\pi\omega d(\varepsilon_2)^{1/2}$ is the complex phase change related to the absorption in the crystal layer with the thickness d.

Reflectance, R, is given with:

$$R = |R_A|^2 \quad (2)$$

The dielectric function of the Cr_2O_3 crystal layer is:

$$\varepsilon_2(\omega) = \varepsilon_\infty \left(1 + \sum_{k=1}^{n} \frac{\omega_{LOk}^2 - \omega_{TOk}^2}{\omega_{TOk}^2 - \omega^2 - i\gamma_{TOk}\omega} - \frac{\omega_P^2}{\omega(\omega + i\Gamma)}\right) \quad (3)$$

Here, ωTO and ωLO represent the transverse and longitudinal optical bulk phonon frequencies, respectively; ε_∞ denotes the high-frequency dielectric constant; ωP is the plasma frequency; and γ and γP are the damping constants for phonons and plasmons, respectively. Surface phonons can be treated analogously to phonons in infinite crystals, with wave functions adjusted to the particle's geometry. The dielectric function of the glass substrate follows the form of equation (2), but without the plasma term.

The far-infrared spectra of Cr_2O_3 thin films, in the spectral range of 60 - 670 cm, at room temperature, are presented in the Fig. 6. The experimental data are presented by circles, while the solid lines are obtained by the theoretical model.

Fig. 6 reveals that the dominant features in all spectra are primarily attributed to the glass substrate. While the addition of the Cr_2O_3 film introduces noticeable changes, these modifications are partially obscured by the substrate's spectral contribution.

The calculated spectrum of glass substrate, presented by red solid line in Fig. 6, was obtained using the eq. (3) without the plasma contribution. As a result of the best fit, we obtained four modes, whose characteristic frequencies were ωTO_1 = 210 cm^{-1}, ωTO_2 = 392 cm^{-1}, ωTO_3 = 435 cm^{-1}, and ωTO_4 = 475 cm^{-1}. Frequency values of these modes have remained the same during the fitting procedure for all Cr_2O_3 thin film samples.

In addition to the characteristics of the glass, for each spectrum we took the required number of IR active modes determined by DFT analysis. The calculated far – infrared reflectivity spectra of Cr_2O_3 thin films on glass substrate are shown as solid lines in the Fig. 6. The results of the numerical fitting of the experimental date according to the model described by eq. 2-4, along with DFT predictions, are presented in Table 2. As can be seen, experimental and theoretical spectra show an excellent match.

In addition to the phonon characteristics presented in Figs. 5 and 6, and confirmed by DFT analysis, the spectrum in Fig. 6 also displays a feature around 130 cm^{-1}, which lies outside the typical phonon range. We interpret this as a surface optical (SO) mode. Surface optical phonon modes can appear in systems where the particle size is considerably smaller than the wavelength of the incident light source [23]. Although SO phonons resemble bulk phonons conceptually, their vibrational amplitudes are confined near the surface of the material, decaying exponentially with distance from the surface.

There are two main types of SO phonon modes based on penetration depth: macroscopic and microscopic. Macroscopic SO modes can include both optical and acoustic frequencies [28]. In isotropic elastic media, acoustic SO modes propagate along the surface or interface, with particle displacements occurring within the sagittal plane—defined by the surface normal and the propagation direction [29]. These modes decay exponentially into the bulk, with penetration depth proportional to the wavelength in the long-wave limit. Unlike acoustic modes, the Fuchs-Kliewer phonon is associated with a macroscopic electric field [30]. Its frequency is determined by solving the Laplace equation for the electrostatic potential in an ionic crystal under appropriate electromagnetic boundary conditions, falling between the transverse optical (TO) and longitudinal optical (LO) phonon frequencies.

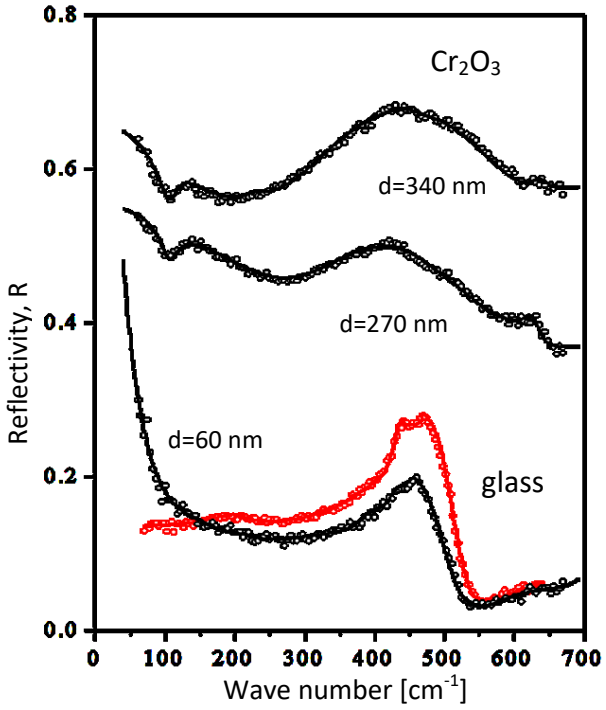

Fig. 6. Far – infrared reflection spectra of Cr_2O_3 thin films with thickness of 60 nm, 270 nm and 340 nm, and the glass substrate. The experimental spectra are presented by circles while solid lines are calculated spectra obtained by a fitting procedure based on the model given by eq. (2) - (4) (colour online)

Given that the observed SO phonon mode in our sample appears around 130 cm^{-1}, below the optical frequency range, we conclude that it corresponds to an acoustic SO mode. This also explains why this SO phonon is detected only in far-infrared meas-urements and not in Raman spectroscopy.

4. Conclusions

Chromium (III) oxide (Cr_2O_3) thin films of varying thicknesses were successfully deposited on glass substrates using the reactive sputtering technique, achieving stable and homogeneous growth. Atomic force microscopy (AFM) confirmed that the films exhibit smooth surfaces with controlled roughness, which is essential for optoelectronic applications.

The phonon properties of the films were investigated through a combination of Raman and far-infrared (FIR) spectroscopy, with additional validation provided by density functional theory (DFT) calculations. A numerical model was employed to simulate the reflectivity spectra of the film–substrate system, showing excellent agreement with experimental measurements.

A particularly significant finding is the identification of the surface optical phonon (SOP) mode in the FIR region. This mode becomes dominant in reduced-dimensional systems, reflecting strong surface and confinement effects. The presence of such a mode marks an important step toward understanding the phonon behavior in thin transition-metal oxide films and its impact on material functionality.

These results demonstrate that Cr_2O_3 thin films, with tunable properties via oxygen partial pressure during deposition, represent a promising material platform for integration into advanced infrared optoelectronic components, including thermal photodetectors, IR sensors, and future photonic devices. Their structural stability, controllable growth, and distinctive phonon features make them particularly well-suited for use in demanding operational environments and integration with existing technological platforms.

Future work should include the integration of Cr_2O_3 thin films into device-relevant architectures, such as heterojunctions, Schottky-type structures, or multilayer infrared platforms, in order to directly correlate the present phononic and optical results with detector and sensor performance, including responsivity, stability, and spectral selectivity.

Acknowledgement

This research was supported by the Science Fund of the Republic of Serbia, Grant No. 7504386, Nano Object in Own Matrix-Self Composite (NOOM-SeC).

References

[1] J. J. Quinn, K.-S. Yi, Springer, Cham (2018).
[2] R. Machkih, B. Ahmed, A. Echchelh, A. Chemsi, Coatings **14**(9), 1088 (2024).
[3] D. K. Sharma, S. Shukla, K. K. Sharma, V. Kumar, Mater. Today **49**(8), 3028 (2022).
[4] A. Chaves, J. G. Azadani, H. Alsalman, D. R. da Costa, R. Frisenda, A. J. Chaves, S. H. Song, Y. D. Kim, D. He, J. Zhou, A. Castellanos-Gomez, F. M. Peeters, Z. Liu, C. L. Hinkle, S.-H. Oh, P. D. Ye, S. J. Koester, Y. H. Lee, Ph. Avouris, X. Wang, T. Low, 2D Materials and Applications **4**, 29 (2020).
[5] C.-Y. Hsu, Z. H. Mahmoud, S. Abdullaev, F. K. Ali, Y. A. Naeem, R. M. Mizher, M. M. Karim, A. S. Abdulwahid, Z. Ahmadi, S. Habibzadeh, E. Kianfar, Case Studies in Chemical and Environmental Engineering **9**, 100626 (2024).
[6] Y. Wang, B. Chen, X.-Z. Wang, M. Chen, S. Li, G. Bai, J. Li, W. Gong, Corrosion Science **217**, 111099 (2023).
[7] J. Singh, P. Bhardwaj, R. Kumar, V. Verma, J. Electron. Mater. **53**, 7179 (2024).
[8] Z. Li, B. Mi, X. Ma, P. Liu, F. Ma, K. Zhang, X. Chen, X. Zhu, Y. Meng, H. Lu, W. Li, Vacuum **228**, 113518 (2024).
[9] M. Sadullah, S.M. Hussain, K. Ghosh, Silicon **16**, 1893 (2024).
[10] Prathiksha, K.A. Jagadish, D. Kekuda, Mater. Res. Express **11**, 105901 (2024).
[11] H. Cao, X. Qiu, Y. Liang, M. Zhao, Q. Zhu, Appl.

Phys. Lett. **88**, 241112 (2006).
[12] V. K. Vashistha, R. Bala, A. Mittal, D. K. Das, R. Pullabhotla, J. Indian Chem. Soc. **100**(8), 101069 (2023).
[13] Z. Pei, X. Zeng, Z. Li, J. Nanosci. Nanotechnol. **16**(5), 4655 (2016).
[14] L. Shaker, A. Al-Amiery, W. Isahak, Green Technologies for Sustainability **2**, 10011 (2024).
[15] L. Chen, M. Hu, J. Feng, Materials Today Physics **35**, 101118 (2023).
[16] D. S. Chuu, C. M. Dai, W. F. Hsieh, C. T. Tsai, J. Appl. Phys. **69**, 12 (1991).
[17] A. Singh, B. Satpati, P. V. Satyam, A. Roy, Journal of Physics: Condensed Matter **17**, 5967 (2005).
[18] M. Gilić, J. Trajić, N. Romčević, M. Romčević, D. V. Timotijević, G. Stanišić, I. S. Yahia, Opt. Mater. **35**, 1112 (2013).
[19] P. Giannozzi, S. Baroni, N. Bonini, M. Calandra, R. Car, C. Cavazzoni, D. Ceresoli, G. L. Chiarotti, M. Cococcioni, I. Dabo, Journal of Physics: Condensed Matter **21**, 395502 (2009).
[20] P. E. Blöchl, Phys. Rev. B **50**, 17953 (1994).
[21] G. Kresse, D. Joubert, Phys. Rev. B **59**, 1758 (1999).
[22] M. Gilić, R. Kostić, D. Stojanović, M. Romčević, B. Hadžić, M. Petrović, U. Ralević, Z. Lazarević, J. Trajić, J. Ristić-Djurović, J. Ćirković, N. Romčević, Optical and Quantum Electronics **50**, 288 (2018).
[23] J. P. Perdew, K. Burke, M. Ernzerhof, Phys. Rev. Lett. **77**, 3865 (1996).
[24] A. I. Liechtenstein, V. I. Anisimov, J. Zaanen, Phys. Rev. B **52**, R5467 (1995).
[25] T. Larbi, B. Ouni, A. Gantassi, K. Doll, M. Amlouk, T. Manoubi, J. Magn. Magn. Mater. **444**, 16 (2017).
[26] A.S.O. Gomes, N. Yaghini, A. Martinelli, E. Ahlberg, J. Raman Spectrosc. **48**(10), 1256 (2017).
[27] M. Gilić, M. Petrović, R. Kostić, D. Stojanović, T. Barudžija, M. Mitrić, N. Romčević, U. Ralević, J. Trajić, M. Romčević, I. S. Yahia, Infrared Physics & Technology **76**, 276 (2016).
[28] J. Mitrić, N. Paunović, M. Mitrić, B. Vasić, U. Ralević, J. Trajić, M. Romčević, W. D. Dobrowolski, I. S. Yahia, N. Romčević, Physica E **104**, 64 (2018).
[29] R. Fuchs, K. L. Kliewer, Phys. Rev. **140A**, 2076 (1965).
[30] R. F. Wallis, Surface Science **299/300**, 612 (1994).

*Corresponding author: milicap@ipb.ac.rs